

# SpikySpace: A Spiking State Space Model for Energy-Efficient Time Series Forecasting

Kaiwen Tang, Jiaqi Zheng, Yuze Jin, Yupeng Qiu, Guangda Sun, Zhanglu Yan\*, Weng-Fai Wong

*School of Computing*

*National University of Singapore*

Singapore, Singapore

{tang\_kaiwen, jiaqi, jin.yuze, qiu\_yupeng, guangda, e0385109}@u.nus.edu, wongwf@comp.nus.edu.sg

**Abstract**—Time-series forecasting often operates under tight power and latency budgets in fields like traffic management, industrial condition monitoring, and on-device sensing. These applications frequently require near real-time responses and low energy consumption on edge devices. Spiking neural networks (SNNs) offer event-driven computation and ultra-low power by exploiting temporal sparsity and multiplication-free computation. Yet existing SNN-based time-series forecasters often inherit complex transformer blocks, thereby losing much of the efficiency benefit. To solve the problem, we propose SpikySpace, a spiking state-space model (SSM) that reduces the quadratic cost in the attention block to linear time via selective scanning. Further, we replace dense SSM updates with sparse spike trains and execute selective scans only on spike events, thereby avoiding dense multiplications while preserving the SSM’s structured memory. Because complex operations such as exponentials and divisions are costly on neuromorphic chips, we introduce simplified approximations of SiLU and Softplus to enable a neuromorphic-friendly model architecture. In matched settings, SpikySpace reduces estimated energy consumption by 98.73% and 96.24% compared to two state-of-the-art transformer based approaches, namely iTransformer and iSpikformer, respectively. In standard time series forecasting datasets, SpikySpace delivers competitive accuracy while substantially reducing energy cost and memory traffic. As the first full spiking state-space model, SpikySpace bridges neuromorphic efficiency with modern sequence modeling, marking a practical and scalable path toward efficient time series forecasting systems.

**Index Terms**—Time Series Forecasting, Spiking Neural Networks, State Space Model, Energy Consumption

## I. INTRODUCTION

Edge-deployed time-series analytics systems, such as urban traffic management, industrial condition monitoring, and on-device wearable sensing, are driving a need for time-series forecasting methods that operate on the edge. Due to privacy, reliability or bandwidth constraints, these tasks must produce real-time predictions locally without relying on the cloud. While deep learning methods including RNNs, LSTMs, and GRUs or more recently transformer-based structures can achieve high accuracy, they still remain much energy hungry according to complex multiplication and exponentiation operations. To meet the energy and latency demands, Spiking Neural Networks (SNNs), which adopts the event-driven paradigm and only adapt simpler addition and shifting operations,

has emerged as a promising direction towards edge intelligence [1]. This mechanism allows compute and memory activity to scale with signal changes rather than sequence length, enabling low-latency operation on edge devices. Furthermore, SNNs possess an intrinsic ability to model temporal dynamics through membrane potentials and spike timing, making it well-suited for streaming time-series forecasting in scenarios like sensor-based monitoring and edge-level control, where both energy efficiency and real-time responsiveness are critical.

However, most recent SNN works focus on better performance on time series tasks instead of energy efficiency. Works like SpikeTCN [2], iSpikformer [2], and TS-LIF [3] have achieved desirable performance, while they still rely on high-cost encoders or the transformer architecture, whose attention mechanism remains energy-intensive due to frequent memory access and global communication, even under spiking implementations. Although these previous works achieved desirable performance, their improvements often come at the cost of increased energy consumption. While pursuing higher accuracy is important, edge-deployed forecasting systems must ultimately balance accuracy against deployability. These limitations highlight the need for a more energy-efficient neuromorphic time-series model that achieves competitive predictive performance under stringent energy and memory constraints.

In this work, we propose SpikySpace, a novel spiking model for time series forecasting that addresses the imbalance between accuracy and energy efficiency in prior spiking approaches. SpikySpace adopts an event-driven state space architecture that combines selective spike-based updates with continuous time dynamics, allowing it to model temporal dependencies efficiently under strict power and memory constraints. Through the joint optimization of structural sparsity and spike-driven state transitions, SpikySpace achieves accuracy comparable to or better than existing models while greatly reducing power consumption.

Specifically, in SpikySpace, we leverage the *state-space model* (SSM) [4], [5] formulation to replace the high computational cost of the transformer while maintaining its strong modeling capacity. Instead of relying on sequential hidden-state updates as in RNNs, LSTMs, and GRUs, or on dense self-attention and large context buffers as in transformers, SSMs represent temporal dynamics through compact latent states updated via linear-time recurrences. This formulation

\*Corresponding author

allows information to propagate over long horizons with  $O(L)$  complexity, significantly reducing both computation and memory costs compared to the  $O(L^2)$  attention in transformers and avoiding the sequential bottleneck of recurrent networks. By embedding this formulation into an event-driven spiking framework, SpikySpace inherits the long-range dependency modeling of SSMs while maintaining the sparse and energy-efficient computation of SNNs. Consequently, SpikySpace matches transformer-level forecasting performance with far lower energy consumption, making it well-suited for deployment on neuromorphic or edge platforms.

Developing SSM-based SNNs remains challenging due to the limited explore of fully spiking state updating as well as the complex activation functions involved. SpikySpace optimize the nonlinearities such as SiLU and Softplus employed in gating and readout in modern SSMs for neuromorphic hardware compatibility. We first develop SNN-compatible approximations for Softplus and SiLU with power-of-two components and linear transformations, namely PTsoftplus and PTSiLU. We theoretically prove our proposed components are continuously differentiable and act close to the original functions. This design allows the activation to be implemented through efficient bit-shifting operations, removing costly divisions and exponentials while preserving smooth gating behavior. For training, we first learn a quantized ANN in the continuous domain using the proposed PTsoftplus and PTSiLU approximations under low-bit constraints for activations. We then perform a deterministic ANN to SNN conversion that maps the quantized activations, gates, and state updates to spike events. The resulting SpikySpace is a spiking forecaster suitable for resource-constrained edge deployment. While several prior efforts have attempted to integrate SNNs and SSMs [6]–[9], their formulations still partly rely on dense multiplications and retain complicated activations such as Softplus or SiLU, limiting their spiking sparsity and hardware efficiency.

Evaluated on four multivariate forecasting datasets, SpikySpace achieves competitive or superior accuracy while substantially reducing parameter size and energy consumption. Specifically, on datasets like Metr-la and Electricity [10], [11], SpikySpace attains average  $R^2$  scores of 0.778 and 0.992, surpassing the accuracy of the previous best-performing SNN SpikeSTAG by 3.3% and 0.7%, respectively, while consuming only 2.7% of its energy. SpikySpace also achieves the energy savings by  $26.58\times$  over iSpikformer and  $78.9\times$  over iTransformer, without compromising accuracy stability. We further conduct ablation studies on the proposed PTsoftplus and PTSiLU and spiking timesteps, verifying their contribution and justify our parameter selection. Mechanistically, SpikySpace retains information over long horizons through its explicit latent state, while event-driven spikes naturally skip redundant updates. The result shows that structured spiking state evolution enables efficient and scalable time-series forecasting on neuromorphic and edge devices.

Our main contributions are summarized as follows:

- We present SpikySpace, a hardware-friendly model for time series tasks implemented using a fully spiking state

model. To our knowledge, SpikySpace is the first fully spiking SSM, where both the latent state updates and non-linear transformations are realized through discrete spike-driven computation. This makes it exceptionally energy-efficient and inherently compatible with neuromorphic hardware.

- We propose lightweight approximations for SiLU and Softplus, enabling full compatibility with neuromorphic hardware, removing a major obstacle to deploying SSM-based SNNs on energy constraint systems.
- SpikySpace achieves competitive or superior forecasting accuracy while drastically reducing energy consumption and parameter size compare with the state-of-the-art methods, demonstrating a highly favorable balance between accuracy and efficiency for neuromorphic and edge deployment.

## II. RELATED WORK

### A. Spiking Neural Networks

Spiking neural networks (SNNs) consist of interconnected spiking neurons that communicate through discrete spike events, enabling energy-efficient and event-driven computation [12], [13]. A spiking neuron integrates incoming signals over time and emits a spike once its “membrane potential” exceeds a threshold, mimicking the behavior of biological neurons. Because information is represented as discrete spike events rather than continuous activations, computation only occurs when events happen, leading to lower energy consumption and improved efficiency. Moreover, owing to their temporal coding mechanism, SNNs are particularly well-suited for modeling temporal or sequential signals. Such network architectures have been extensively explored across various tasks, ranging from image classification and natural language processing to autonomous control [14]–[18].

Although many SNN architectures employ transformer-style self-attention blocks to exploit long-range dependencies, the underlying attention mechanism still imposes a quadratic complexity barrier in sequence length. To address this limitation, a growing line of research has explored State-Space Models (SSMs) such as S4 and Mamba as efficient alternatives to attention. These models achieve linear-time (or near-linear) complexity and enable fully parallel updates with respect to input length [4], [5].

To capture long-range dependencies, many SNN architectures often utilise transformer-like self-attention mechanisms. However, the attention operation involves quadratic computational and memory complexity with respect to sequence length, and the dense all-to-all interactions are not well aligned with the sparse and event-driven nature of SNNs, causing suboptimal efficiency. Alternative architectures such as State Space Models (SSMs), including S4 and Mamba [4], [5], provide linear-time sequence modeling and parallel updates, but adapting these continuous-time formulations to the spiking domain remains non-trivial challenges.

### B. Challenges of Adapting SSMs to SNNs

Structured SSM architectures are originally designed for conventional artificial neural networks (ANNs). Their architectures and operations are not directly compatible with SNNs. SSM-based layers typically rely on real-valued state vectors that evolve at every discrete time step or through continuous differential equations and use dense linear algebra operations such as matrix multiplications and convolutions. In contrast, SNNs operate in an event-driven manner with binary spikes and sparse, asynchronous updates. The continuous-time dynamics and long convolutions of SSMs do not naturally align with this spike-driven computation model.

There have been some explorations of integrating SNNs with SSMs. Existing studies [6]–[9] have made progress toward spiking variants of SSMs. However, their formulations still rely on continuous states and dense multiplication operations, which prevent them from fully exploiting the sparsity and event-driven benefits of spiking computation. Additionally, many of these designs treat SNNs merely as wrappers or feature extractors around conventional SSM blocks. Complex activation functions and operations used in SSMs, such as SoftPlus and SiLU, are retained in a continuous manner.

Overall, current solutions fail to achieve a genuinely end-to-end, fully spiking state-space model in which the latent state is inherently updated by sparse spike activity.

In SpikySpace, we address this gap by exploring how the principled dynamics of SSMs can be adapted to the spiking regime, paving the way for a Spiking SSM architecture that combines the long-range modeling capability of SSMs with the efficiency of event-driven SNN computation.

### C. Time-series Forecasting

Time-series forecasting aims to predict future values based on historical sequences. It serves as a fundamental technique across diverse domains, including finance, healthcare, and industrial monitoring.

Classical statistical methods such as ARIMA [19] and exponential smoothing [20] capture trend and seasonality under stationarity assumptions, but struggle with nonlinear dynamics, regime shifts, and long-range dependencies in multivariate settings.

Neural networks such as LSTMs [21] and GRUs [22] improve the modeling of sequential dependencies but can be computationally intensive for long sequences. Temporal convolutional networks (TCNs) [23] enlarge receptive fields through dilation and allow parallel training, but require deep stacks or large kernels to capture long-range contexts. Transformers have also been applied to time-series forecasting. Variants such as Informer [24] and Autoformer [25] reducing computation through sparse attention or decomposition strategies and show strong accuracy on long-horizon benchmarks [26]. However, these models remain memory-bound due to key-value caches and dense step-wise updates.

Complementary efficiency techniques for neural networks, such as quantization, pruning, lightweight backbones, and mixed precision, can reduce arithmetic cost and memory

footprint. However, the *dense* computation pattern remains a fundamental limitation: compute and memory traffic still scale with sequence length rather than information content [27]. As a result, throughput and latency remain sensitive to context windows and key-value caches even after compression, particularly in streaming or on-device settings.

To enable truly efficient forecasting, recent studies have explored SNNs for sequential and multivariate prediction, leveraging event-driven sparsity to align computation with informative temporal changes [2], [3], [28], [29]. Recurrent and convolutional spiking models capture local dynamics with sparse updates, while spiking Transformers introduce positional or relative attention to model longer-range dependencies. Graph-based spiking architectures have also been proposed to exploit spatial correlations in sensor networks [28], [29].

However, these approaches often retain per-timestep (or per-node) dense operations at some stage of the pipeline and trade accuracy for sparsity on long horizons. This motivates our direction: combining the structured memory of state-space models with *event-triggered* execution, so that updates are driven by spike activity rather than timestamp, preserving long-range accuracy while achieving sparse, and information-aligned computation.

## III. PRELIMINARY

### A. Problem Statement

**Definition 1 (Multivariate Time Series):** A multivariate time series is an ordered sequence of observations  $X = \{x_1, x_2, \dots, x_{|X|}\} \in \mathbb{R}^{|X| \times N}$ , where  $N$  is the number of variables and each observation  $x_i \in \mathbb{R}^N$  represents the values of all variables at time step  $i$ . Given a historical window  $X_H \in \mathbb{R}^{H \times N}$ , the goal is to forecast the next  $G$  steps. The target sequence is  $X_G \in \mathbb{R}^{G \times N}$  that represents the future states of all variables. During training,  $(X_H, X_G)$  pairs are sampled from historical data for the model to learn temporal dependencies. During inference, an observed series  $X_O \in \mathbb{R}^{O \times N}$  is provided, and the model produces predictions for the next  $G$  steps. In this work, the mapping  $X_H \mapsto X_G$  is implemented by an SNN, which performs event-driven updates for efficient computation on streaming time-series data.

### B. Spike Neuron Model

SNNs communicate via discrete spikes rather than continuous activation, leading to event-driven and temporally sparse computation. However, training SNNs is non-trivial because the spike generation function is inherently non-differentiable, which makes gradient-based optimization inapplicable. To overcome this, two main strategies are commonly employed. The first relies on *surrogate gradients* [30], which approximate the gradients of spike events to allow backpropagation. The second, *ANN-to-SNN conversion* [31], leverages a pre-trained artificial neural network (ANN) and maps its continuous neuron activations to spiking dynamics, producing a functionally similar SNN. In this work, we follow the ANN-to-SNN conversion approach to construct our SpikySpace.

Among spiking neuron models, the *Integrate-and-Fire* (IF) neuron is widely used for its simplicity and efficiency [32]. In the IF model, a neuron's membrane potential  $V(t)$  integrates incoming synaptic currents over time:

$$\frac{dV(t)}{dt} = I_{\text{syn}}(t), \quad (1)$$

where  $I_{\text{syn}}(t)$  denotes the total synaptic input. When the potential  $V(t)$  surpasses a threshold  $\theta$ , the neuron emits a spike and resets. We adopt an optimized version called *Average Integrate-and-Fire* [33], which reduces memory access by accumulating inputs and updating the potential in a single step, requiring only one read of the synaptic weights per time step. We provide the detailed spike generation method we adopted in algorithm 1.

---

#### Algorithm 1 Average IF model

---

```

1: Input: Weight  $w_{ij}^l$  of layer  $l$  from neuron  $i$  to neuron  $j$ , bias  $b_i^l$ , input spike train  $s_i^l$ , threshold  $\theta$ , membrane potential  $U_i^l(t)$  at timestep  $t$ , time window size  $T$ ;
2: Output: Spike train  $s_j^l$ ;
3:  $U_i^l(t) \leftarrow \sum_j (w_{ij}^l \cdot s_i^l(t) + b_i^l)$ 
4:  $A_i^l \leftarrow \sum_{t=1}^T U_i^l(t)/T$ 
5:  $s_i^l(0) \leftarrow 0$ ,  $V_i^l(0) \leftarrow 0$ ;
6: for  $t \leftarrow 1$  to  $T$  do
7:    $V_i^l(t) \leftarrow V_i^l(t-1) + A_i^l$ 
8:    $s_j^{l+1}(t) \leftarrow \begin{cases} 1, & V_i^l(t) \geq \theta \\ 0, & \text{otherwise} \end{cases}$ ;
9:    $V_i^l(t) \leftarrow \begin{cases} V_i^l(t) - \theta, & V_i^l(t) \geq \theta \\ V_i^l(t), & \text{otherwise} \end{cases}$ .
10: end for
11: return  $s_j^{l+1}$  {Output the ASG spike train of neuron  $i$ }
```

---

### C. State Space Model

State Space Models (SSMs) provide a compact, physics-inspired way to model sequence dynamics by evolving a low-dimensional latent state and mapping it to observable outputs. Compared with generic recurrent architectures, SSMs admit exact continuous-to-discrete conversions and an analytic convolutional kernel, which together enable numerically stable long-horizon reasoning and efficient implementations.

A continuous-time linear SSM is given by

$$\frac{dx(t)}{dt} = Ax(t) + Bu(t), \quad (2)$$

$$y(t) = Cx(t) + Du(t), \quad (3)$$

where  $x(t) \in \mathbb{R}^N$  is the hidden state,  $u(t) \in \mathbb{R}^m$  is the input,  $y(t) \in \mathbb{R}^p$  is the output, and  $A, B, C, D$  are system matrices defining state dynamics and input/output mappings. Discretizing with time step  $\Delta t$  yields

$$x_{n+1} = A_d x_n + B_d u_n, \quad (4)$$

$$y_n = C x_n + D u_n, \quad (5)$$

where  $A_d$  and  $B_d$  are the discrete-time equivalents of  $A$  and  $B$ , and  $n$  indexes the time step. This formulation allows the system to capture temporal dependencies over long sequences: the output  $y_n$  can be expressed as a convolution of the input sequence  $u$  with an effective kernel

$$y_n = \sum_{k=0}^n K_k u_{n-k}, \quad \text{with } K_k = C A_d^k B_d. \quad (6)$$

Thus, SSMs provide a principled way to model long-range temporal dependencies while maintaining a compact state representation.

## IV. METHOD

### A. Overall Framework

Our proposed SpikySpace model is illustrated in Fig. 1. It consists of a residual block, a state space module and a forecasting head. To be specific, it employs a pre-normalization structure, utilizing RMSNorm before the Spiking Mamba unit designed for time series forecasting to stabilize the training dynamics. Thus, it can be represented as:

$$\mathbf{y} = \mathbf{x} + \text{SpikingMamba}(\text{RMSNorm}(\mathbf{x})) \quad (7)$$

Within each Spiking Mamba block, we first expand the feature dimension from the number of variance  $d_v$  to  $2d_{\text{hidden}}$  via an input projection, splitting the output into a data path  $\mathbf{x}_{\text{in}}$  and a residual gate path  $\mathbf{x}_{\text{res}}$ . Here, we denote  $d_v$  as the number of variants, using as the input dimension, while  $d_{\text{hidden}}$  is the hidden size of the model. In our model, we set the hidden size as a small value to downsize the parameter size. After feature extraction, the data path  $\mathbf{x}_{\text{proj}}$  is processed by our spiking SSM block for global dependency capture.

After the spiking SSM blocks, the final feature representation  $\mathbf{Z} \in \mathbb{R}^{B \times L \times D_v}$  is permuted and passed through a linear layer as a forecasting head to map the input window length  $L_{\text{in}}$  to the required prediction horizon  $L_{\text{out}}$ .

To align computation with spike events, activations are quantized and converted into equivalent spike trains, and the corresponding matrix-vector product becomes an accumulation over spike indices. This design removes high-cost multiplications with accumulation and lets compute traffic scale with firing rate rather than wall-clock sequence length.

Furthermore, expensive exponentials or divisions in standard activations are replaced by piecewise linear or power-of-two approximations of Softplus and SiLU, which are natively supported on neuromorphic substrates via additions and bit-shifts. Overall, our design provides fixed-latency streaming updates, a constant-size state independent of  $L$ , and an energy profile that closely tracks the number of synaptic operations.

### B. State Space Module

The key to SpikySpace's efficiency is the integration of the Spike Neuron into the core of the SpikingMamba, fundamentally transforming the continuous-time system into a sparse, event-driven mechanism. Our SSM unit is responsible for the global sequence modeling within SpikingMamba.

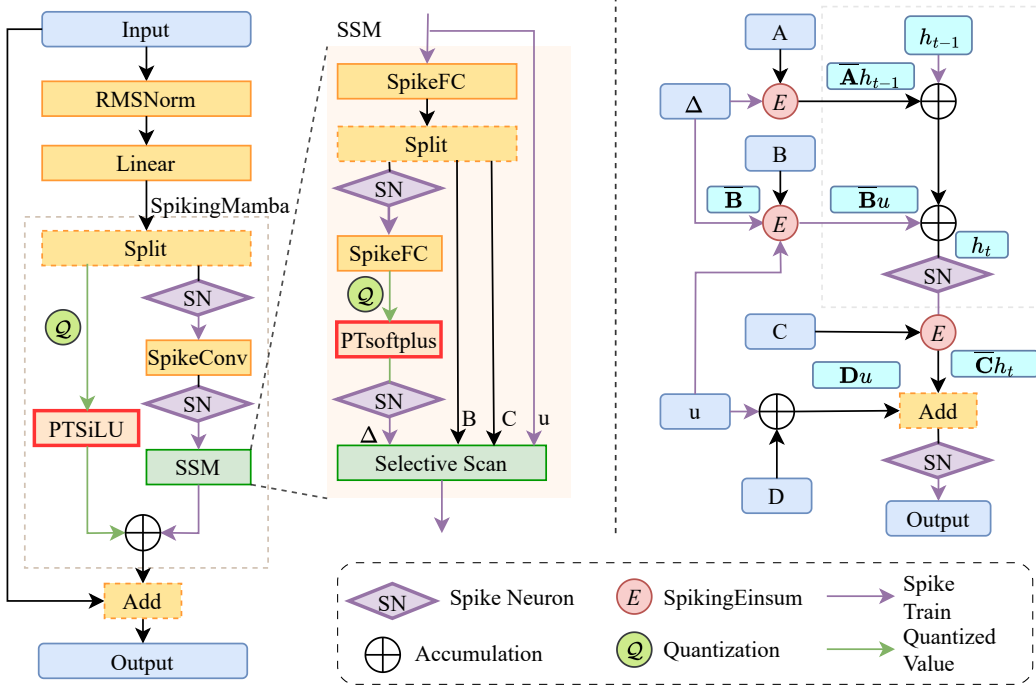


Fig. 1: Overall structure of SpikySpace. Left: The structure of SpikingMamba; Right: Selective Scan

1) *Local Convolutions with Spiking Activation*: Before entering the SSM block, the data path  $x_{in}$  undergoes depth-wise separable 1D convolution to capture the local temporal feature. Crucially, the non-linear activation following the convolution is replaced by a spike neuron, denoted as  $\mathcal{SN}(\cdot)$ , which transforms the continuous feature  $x_{in}$  into a sparse, binary spike train  $s \in \{0, 1\}$  over  $T$  timesteps:

$$s_{in} = \mathcal{SN}(x_{in}), \quad (8)$$

$$s = \mathcal{SN}(\text{Conv1D}(s_{in})), \quad (9)$$

where Conv1D denotes a depthwise convolution applied independently to each latent channel.

2) *Spiking SSM*: Then we input  $s$  into the SSM block. We use the SSM block to model long-range temporal dependencies through a continuous-time state evolution. Given the input spike train  $s$ , it learns a latent dynamical system parameterized by  $(\Delta, A, B, C, D)$ , where  $\Delta$  controls the discrete time step and  $(A, B, C, D)$  define the system dynamics. Through iterative state updates, the SSM propagates information efficiently over long horizons. Before the selective scan, we derive the step size and dynamic parameters as follows.

After a linear transformation, we expand the input and split it into step-size  $\Delta$  and learnable weight matrix  $B, C$ . As  $\Delta$  is going to be send to a fully connection layer, we also encode it into a spike train. Then we quantize the output into integers to send into our proposed PTSoftplus to get the  $\Delta$  we send into the selective scan block.

Thus, the process can be represented as:

$$\begin{aligned} A, B, C &= \text{Split}(Ws + b), \quad \Delta_s = \mathcal{SN}(\Delta), \\ \tilde{\Delta} &= Q(W_{\Delta}\Delta_s + b_{\Delta}), \\ \Delta &= \text{PTSoftplus}(\tilde{\Delta}), \quad \Delta_s = \mathcal{SN}(\Delta), \end{aligned} \quad (10)$$

where PTsoftplus is our approximation to replace the complicated activation function Softplus which will be introduced in Section IV-C and  $Q$  representing a quantization process to ensure the input of PTsoftplus is an integer.

Meanwhile, the SSM's diagonalizable dynamics parameters are learned as

$$A = -\exp(A_{\log}) \in \mathbb{R}^{d_{\text{hidden}} \times n}, \quad D \in \mathbb{R}^{d_{\text{hidden}}} \quad (11)$$

Here,  $A_{\log}$  denotes the logarithm of a trainable parameter  $A$ . Since  $A_{\log}$  is fixed after training, its exponential counterpart  $-\exp(A_{\log})$  can be pre-computed, incurring no extra overhead during inference. Then,  $\{\Delta, A, B, C, D\}$  will be send to the selective scan module.

3) *Spike-Driven Selective Scan Module*: With the learned parameters and step size, the SSM then performs a spike-driven selective scan to iteratively update the latent state.

In the original Mamba formulation, the transition matrix is obtained through an exponential operation:

$$\bar{A}_t = \exp(\Delta_t A) \quad (12)$$

To facilitate hardware efficiency, we approximate the exponential with a power-of-two representation and round the input to integers, which allows efficient bit-shifting implementation:

$$\bar{A}_t = 2^{\lfloor \Delta_t A \rfloor} \quad (13)$$

---

**Algorithm 2** SpikingMamba with Selective Scan

---

- 1: **Input:** Spike train  $\mathbf{s} \in \mathbb{R}^{B \times L \times d}$ ; hidden dimension  $d_{\text{hidden}}$ ; sequence length  $L$
- 2: **Require:** Linear Projection Weight  $\mathbf{W} \in \mathbb{R}^{d \times (r_B + r_C + r_\Delta)}$ ,  $\mathbf{W}_\Delta \in \mathbb{R}^{r_\Delta \times r_\Delta}$ , Bias  $\mathbf{b} \in \mathbb{R}^{r_B + r_C + r_\Delta}$ ,  $\mathbf{b}_\Delta \in \mathbb{R}^{r_\Delta}$ , SSM dynamics  $\mathbf{A}_{\log} \in \mathbb{R}^{d_{\text{hidden}} \times n}$ ,  $\mathbf{D} \in \mathbb{R}^{d_{\text{hidden}}}$
- 3: **Output:** Predicted Spike Train  $\mathbf{y} = \{\mathbf{y}_t\}_{t=1}^L$
- 4: **Stage 1: Parameters Preparation**
- 5:  $\mathbf{h}_0 \leftarrow \mathbf{0}$  {Initialize the Hidden State}
- 6:  $(\mathbf{\Delta}, \mathbf{B}, \mathbf{C}) \leftarrow \text{Split}(\mathbf{W}\mathbf{s} + \mathbf{b})$
- 7:  $\mathbf{\Delta}_s \leftarrow \mathcal{SN}(\mathbf{\Delta})$
- 8:  $\tilde{\mathbf{\Delta}} \leftarrow \mathcal{Q}(\mathbf{W}_\Delta \mathbf{\Delta}_s + \mathbf{b}_\Delta)$  {Quantize Pre-activation}
- 9:  $\mathbf{\Delta} \leftarrow \mathcal{SN}(\text{PTSoftplus}(\tilde{\mathbf{\Delta}}))$
- 10:  $\mathbf{A} \leftarrow -\exp(\mathbf{A}_{\log})$  {Done during Training stage}
- 11: **Stage 2: Selective Scan**
- 12: **for**  $t = 1$  **to**  $L$  **do**
- 13:    $\bar{\mathbf{A}}_t \leftarrow 2^{\lfloor \mathbf{\Delta}_t \mathbf{A} \rfloor}$  {Power-of-two Transition}
- 14:    $\bar{\mathbf{B}}_t \leftarrow \mathbf{\Delta}_t \mathbf{B}_t$
- 15:    $\mathbf{h}_t \leftarrow \bar{\mathbf{A}}_t \mathbf{h}_{t-1} + \bar{\mathbf{B}}_t \mathbf{s}_t$
- 16:    $\mathbf{h}_t \leftarrow \mathcal{SN}(\mathbf{h}_t)$
- 17:    $\mathbf{y}_t \leftarrow \mathcal{SN}(\mathbf{C}_t \mathbf{h}_t + \mathbf{D} \mathbf{s}_t)$  {Encode Output into Spikes}
- 18: **end for**
- 19: **return**  $\mathbf{y}$

---

The state vector  $\mathbf{h}_t$  acts as the memory. To enforce SNN constraints within the sequential scan loop, we introduce an additional spike neuron after the state update. At each timestep  $t$ , the discrete time dynamics are defined as:

$$\bar{\mathbf{B}}_t = \mathbf{\Delta}_t \mathbf{B}_t, \quad (14)$$

$$\mathbf{h}_t = \mathcal{SN}(\bar{\mathbf{A}}_t \mathbf{h}_{t-1} + \bar{\mathbf{B}}_t \mathbf{u}_t), \quad (15)$$

where  $\mathbf{h}_t \in \mathbb{R}^{B \times d_{\text{hidden}} \times n}$  denotes the hidden state which is encoded into a spike train, and  $\mathbf{s}_t$  is the spiking input at step  $t$ . The module output  $\mathbf{y}_t$  is computed using the  $\mathbf{C}$  matrix and a direct skip connection  $D$ :

$$\mathbf{y}_t = \mathcal{SN}(\mathbf{C}_t \mathbf{h}_t + \mathbf{D} \mathbf{s}_t). \quad (16)$$

This recurrent scanning mechanism allows the model to propagate information over long horizons with linear-time complexity  $O(L)$ , while maintaining spiking sparsity and discrete-time stability. By dynamically adjusting  $\mathbf{\Delta}_t$ , the selective scan adaptively modulates the update rate of each latent dimension, thus achieving efficient state evolution under event-driven constraints. The whole procedure of our SpikingMamba block is shown in Algorithm 2.

4) *Output:* After obtaining the output  $\mathbf{y}$  from the SSM, we further apply a lightweight residual gating module to enhance nonlinearity and stabilize quantized representations. Specifically, we quantize the residual signal, followed by the proposed PTSiLU activation, which will be detailed introduced in IV-D. The processing of  $\mathbf{x}_{\text{res}}$  is represented as:

$$\tilde{\mathbf{x}}_{\text{res}} = \text{PTSiLU}(\mathcal{Q}(\mathbf{x}_{\text{res}})) \quad (17)$$

Then the residual mechanism would accumulate the  $\tilde{\mathbf{x}}_{\text{res}}$  according to the output spike train  $\mathbf{y}$  with as:

$$\tilde{\mathbf{y}} = \mathbf{y} \odot \tilde{\mathbf{x}}_{\text{res}}, \quad (18)$$

where  $\odot$  denotes the element-wise product. The final model output is obtained through a linear projection:

$$\mathbf{z} = \mathbf{W}_o \tilde{\mathbf{y}} + \mathbf{b}_o. \quad (19)$$

where  $\mathbf{W}_o$  is the weight and  $\mathbf{b}_o$  is the bias of the output forecasting head. Note that although the input to the final forecasting head,  $\tilde{\mathbf{y}}$ , is not explicitly encoded as spike trains, it is derived from the element-wise product between a spike train and the output of the PTSiLU activation. Since PTSiLU operates on integer valued inputs using power-of-two scaling, its output consists of quantized values that can be efficiently processed through simple accumulation, bit-shifting, and look-up table operations.

The above formulation completes our SpikingMamba block. In the following section, we detail our proposed activation approximations, PTSoftplus and PTSiLU, which replace conventional exponential-based functions with power-of-two formulations, enabling bit-shift implementation on neuromorphic hardware.

### C. Power-of-Two Softplus

The Softplus function is widely used in SSMs such as Mamba, where the non-negativity of state parameters and stable gradient flow are crucial for modeling long-range temporal dynamics. The continuous and differentiable nature of Softplus provides a numerically stable alternative to the hard ReLU. Formally, given an input tensor  $\mathbf{x} \in \mathbb{R}^{B \times T \times D}$ , where  $B$  denotes the batch size,  $T$  the sequence length, and  $D$  the feature dimension, the Softplus activation is defined as:

$$\text{Softplus}(\mathbf{x}) = \ln(1 + e^{\mathbf{x}}). \quad (20)$$

Each element of  $\mathbf{x}$  is independently transformed by this function, producing an output tensor  $\mathbf{y} \in \mathbb{R}^{B \times T \times D}$  with the same shape but strictly positive values.

However, while Softplus offers clear algorithmic advantages, its reliance on exponential and logarithmic operations which is hard to implemented by neuromorphic hardware, making direct applying softplus in SNNs impractical. To address this limitation, we propose *Power-of-Two based Softplus* (PTSoftplus), a piecewise function designed to preserve the smooth and non-negative characteristics of Softplus while substantially reducing computational complexity. This approximation enables efficient and low-power realization of Softplus-like behavior on SNNs and other event-driven hardware, facilitating the deployment of SSMs in energy-constrained neuromorphic environments.

Our approximate Softplus function, PTSoftplus, is defined as the following piecewise function:

$$\text{PTSoftplus}(x) = \begin{cases} 2^x, & \text{if } x < x_c, \\ x + C, & \text{otherwise,} \end{cases} \quad (21)$$

where the parameters

$$x_c = \log_2 \left( \frac{1}{\ln 2} \right) \approx 0.5288,$$

$$C = \frac{1}{\ln 2} - x_c \approx 0.9139.$$

*a) Smoothness and Closeness Analysis:* To ensure the stability of this approximation during gradient descent training, we first prove that  $\text{PTSoftplus}(x)$  is also a continuously differentiable function.

**Lemma 1.**  *$\text{PTSoftplus}$  is continuously differentiable.*

*Proof.* Both  $2^x$  and  $x+C$  are infinitely differentiable on their own. The only point we need to check is  $x = x_c$ .

We first show that the function value is continuous at  $x = x_c$ . The left-hand limit of  $\text{PTSoftplus}$  at  $x = x_c$  is

$$\lim_{x \rightarrow x_c^-} \text{PTSoftplus}(x) = \lim_{x \rightarrow x_c^-} 2^x = 2^{x_c} = \frac{1}{\ln 2},$$

and the right-hand limit at  $x = x_c$  is

$$\lim_{x \rightarrow x_c^+} \text{PTSoftplus}(x) = \lim_{x \rightarrow x_c^+} x + C = x_c + C = \frac{1}{\ln 2}.$$

The left-hand limit equals the right-hand limit, so the  $\text{PTSoftplus}$  function is continuous on  $\mathbb{R}$ .

Next, we show that the first-order derivative of  $\text{PTSoftplus}$  is also continuous at  $x = x_c$ . The derivative of  $\text{PTSoftplus}$  is as follows:

$$\text{PTSoftplus}'(x) = \begin{cases} (\ln 2) \cdot 2^x, & \text{if } x < x_c, \\ 1, & \text{otherwise.} \end{cases}$$

Since the derivative is a constant when  $x \geq x_c$ , we only need to check if the left-hand limit of  $\text{PTSoftplus}'$  at  $x = x_c$  equals 1. The left-hand limit is given by

$$\lim_{x \rightarrow x_c^-} \text{PTSoftplus}'(x) = \lim_{x \rightarrow x_c^-} (\ln 2) \cdot 2^x = (\ln 2) \cdot 2^{x_c}.$$

Substitute  $x_c = \log_2(\frac{1}{\ln 2})$  into the above. Then the value becomes  $(\ln 2) \cdot \frac{1}{\ln 2} = 1$ , which completes the proof.  $\square$

Next, we demonstrate that the proposed  $\text{PTSoftplus}$  function closely approximates Softplus. Specifically, the functional deviation is bounded by a small constant. The derivatives of  $\text{PTSoftplus}$  and Softplus also exhibit pointwise closeness, ensuring the approximation does not detrimentally affect the model's training dynamics.

**Lemma 2.** *The maximum deviation between the  $\text{PTSoftplus}$  and the Softplus function is bounded by 0.914, i.e.*

$$\|\text{PTSoftplus} - \text{Softplus}\|_\infty \leq 0.914.$$

*Moreover, the maximum deviation between the derivatives of  $\text{PTSoftplus}$  and Softplus is bounded by 0.371, i.e.*

$$\|\text{PTSoftplus}' - \text{Softplus}'\|_\infty \leq 0.371.$$

*Proof Sketch..* Define  $f(x) = \text{PTSoftplus}(x) - \text{Softplus}(x)$ . Then the supremum norm of  $f$  (i.e.  $\|f\|_\infty$ ) is the maximum

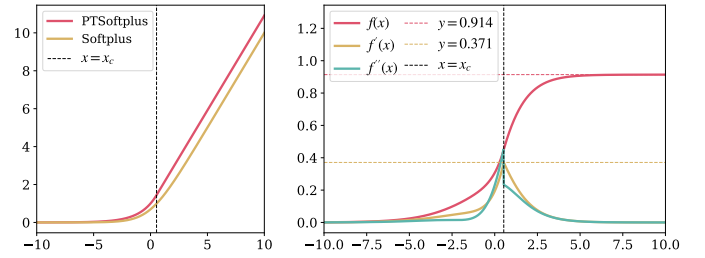


Fig. 2: *Left:* The  $\text{PTSoftplus}$  and the Softplus function. *Right:* The bounds on the deviations between these two functions.

deviation between the function values of  $\text{PTSoftplus}$  and Softplus. Since both functions are continuously differentiable, the function  $f$  is also continuously differentiable. The supremum norm of  $f'$  (i.e.  $\|f'\|_\infty$ ) bounds the maximum difference between the first-order derivative of  $\text{PTSoftplus}$  and Softplus.

As  $x \rightarrow -\infty$ , the value of  $f(x)$  approaches 0, and as  $x \rightarrow \infty$ , the value of  $f(x)$  approaches the constant value  $\frac{1}{\ln 2} - \log_2(\frac{1}{\ln 2})$ . An analysis of the positivity of  $f'(x)$  on the entire domain  $\mathbb{R}$  can show that the function  $f$  is monotonically increasing on  $\mathbb{R}$ . So the value of  $f(x)$  must be between 0 and  $\frac{1}{\ln 2} - \log_2(\frac{1}{\ln 2})$ . That is,

$$\|f\|_\infty = \sup_{x \in \mathbb{R}} |f(x)| \leq \frac{1}{\ln 2} - \log_2(\frac{1}{\ln 2}) \leq 0.914.$$

Since  $f'(x)$  is always positive, to find an upper bound on  $\|f'\|_\infty$ , it suffices to find the maximum value of  $f'(x)$ . It can be shown that, for  $x \geq x_c$ ,  $f'(x)$  is strictly decreasing. Therefore, the maximum value of  $f'(x)$  on  $[x_c, \infty)$  is

$$f'(x_c) = \frac{1}{1 + e^{x_c}} \leq 0.371.$$

On the other hand, an analysis of the positivity of  $f''(x)$  on  $(-\infty, x_c)$  can show that  $f'(x)$  is strictly increasing when  $x < x_c$ . Therefore, we can conclude that the maximum value of  $f'(x)$  on  $\mathbb{R}$  is below 0.371, and consequently

$$\|f'\|_\infty = \sup_{x \in \mathbb{R}} |f'(x)| \leq f'(x_c) \leq 0.371,$$

thereby completing the proof.  $\square$

The detailed proof of Lemma 2 is relegated to the supplementary materials. Fig. 2 visually demonstrates the function shapes and the deviations between the two functions and their respective derivatives.

#### D. Power-of-Two SiLU

The SiLU activation function is a derivative of Softplus and is highly effective in models like Mamba due to its smooth, self-gating properties.

Given an input tensor  $\mathbf{x} \in \mathbb{R}^{B \times T \times D}$ , where  $B$  denotes the batch size,  $T$  the sequence length, and  $D$  the feature dimension, the SiLU activation is defined as:

$$\text{SiLU}(\mathbf{x}) = \mathbf{x} \cdot \text{Sigmoid}(\mathbf{x}). \quad (22)$$

Each element of  $\mathbf{x}$  is independently transformed by this function, producing an output tensor  $\mathbf{y} \in \mathbb{R}^{B \times T \times D}$  with the same shape.

For hardware efficiency, we investigate a simpler piecewise exponential-linear approximation function to SiLU. The proposed activation function, PTSiLU, is defined as:

$$\text{PTSiLU}(x) = \begin{cases} -2^x, & \text{if } x < \bar{x}_c, \\ 2^{-x-1} + x + \bar{C}, & \text{otherwise,} \end{cases} \quad (23)$$

where the parameters

$$\bar{x}_c = \log_2 \left( \frac{\sqrt{1 + 2 \cdot (\ln 2)^2} - 1}{2 \ln 2} \right) \approx -1.7920,$$

$$\bar{C} = -\frac{\sqrt{1 + 2 \cdot (\ln 2)^2}}{\ln 2} - \bar{x}_c \approx -0.2282.$$

*a) Smoothness and Closeness Analysis:* Similar to the PTSoftplus function, to ensure the stability of this approximation during training, we first prove that PTSiLU is also a continuously differentiable function.

**Lemma 3.** PTSiLU is continuously differentiable.

*Proof.* The power functions and  $x$  are all continuously differentiable. So, we only need to check the point  $x = \bar{x}_c$ .

The left-hand limit of PTSiLU at  $x = \bar{x}_c$  is

$$\lim_{x \rightarrow \bar{x}_c^-} \text{PTSiLU}(x) = -2^{\bar{x}_c} = \frac{1 - \sqrt{1 + 2 \cdot (\ln 2)^2}}{2 \ln 2},$$

and the right-hand limit of PTSiLU at  $x = \bar{x}_c$  is

$$\begin{aligned} \lim_{x \rightarrow \bar{x}_c^+} \text{PTSiLU}(x) &= 2^{-\bar{x}_c-1} + \bar{x}_c + \bar{C} \\ &= \frac{\sqrt{1 + 2 \cdot (\ln 2)^2} + 1}{2 \ln 2} - \frac{\sqrt{1 + 2 \cdot (\ln 2)^2}}{\ln 2} \\ &= \frac{1 - \sqrt{1 + 2 \cdot (\ln 2)^2}}{2 \ln 2}. \end{aligned}$$

Since the left-hand limit equals the right-hand limit, the function PTSiLU is continuous.

Next, we show that the derivative of PTSiLU is also continuous. The derivative of PTSiLU is given by

$$\text{PTSiLU}'(x) = \begin{cases} -(\ln 2) \cdot 2^x, & \text{if } x < \bar{x}_c, \\ 1 - (\ln 2) \cdot 2^{-x-1}, & \text{otherwise.} \end{cases}$$

It is easily seen that the derivative is continuous on  $(-\infty, \bar{x}_c)$  and  $[\bar{x}_c, \infty)$ . Therefore, we only need to check the continuity of PTSiLU' at the transition point  $x = \bar{x}_c$ . The left-hand limit of PTSiLU'(x) at  $x = \bar{x}_c$  is

$$\lim_{x \rightarrow \bar{x}_c^-} \text{PTSiLU}'(x) = -(\ln 2) \cdot 2^{\bar{x}_c} = \frac{1 - \sqrt{1 + 2 \cdot (\ln 2)^2}}{2},$$

and the right-hand limit of PTSiLU'(x) at  $x = \bar{x}_c$  is

$$\begin{aligned} \lim_{x \rightarrow \bar{x}_c^+} \text{PTSiLU}'(x) &= 1 - (\ln 2) \cdot 2^{-\bar{x}_c-1} \\ &= 1 - \frac{\sqrt{1 + 2 \cdot (\ln 2)^2} + 1}{2} \\ &= \frac{1 - \sqrt{1 + 2 \cdot (\ln 2)^2}}{2}. \end{aligned}$$

The left-hand limit equals the right-hand limit, so the derivative PTSiLU' is also continuous on  $\mathbb{R}$ .  $\square$

Next, we show that PTSiLU closely approximates SiLU, evidenced by the bounded difference between their function values. Furthermore, the proximity of their first-order derivatives ensures that this approximation does not impair the convergence or stability of the model's training process.

**Lemma 4.** The maximum deviation between the PTSiLU and the SiLU function is bounded by 0.316, i.e.

$$\|\text{PTSiLU} - \text{SiLU}\|_\infty \leq 0.316.$$

Moreover, the maximum deviation between the derivatives of PTSiLU and SiLU is bounded by 0.263, i.e.

$$\|\text{PTSiLU}' - \text{SiLU}'\|_\infty \leq 0.263.$$

*Proof Sketch..* Define  $\bar{f}(x) = \text{PTSiLU}(x) - \text{SiLU}(x)$ . Then the analysis of the deviations between the function values and derivatives of PTSiLU and SiLU reduces to the analysis of  $\bar{f}$  and  $\bar{f}'$ . Given the complexity of PTSiLU, we employ a strategy that is different from the one used in Lemma 1.

We start from the second-order derivative of  $\bar{f}$ , namely  $\bar{f}''$ . A detailed analysis of the terms in  $\bar{f}''(x)$  yields the following upper bound on the absolute value of  $\bar{f}''(x)$ :

$$\sup_{x \in \mathbb{R}} |\bar{f}''(x)| \leq (\ln 2)^2 \cdot 2^{-\bar{x}_c-1} + 0.5 \leq 1.332,$$

which means the rate of change of  $\bar{f}'(x)$  is bounded by the constant value 1.332.

Then, we employ a computer-aided analysis for  $\bar{f}'$  and  $\bar{f}$ . We generate a sequence of points  $\mathcal{X} = \{x_1, x_2, \dots, x_N\}$  from -10 to 10, where  $x_{i+1} - x_i = 0.001$  for  $i = 1, \dots, N - 1$ . Then we compute the value of  $\bar{f}'(x)$  for each  $x \in \mathcal{X}$ . The numerical results show that these values are between -0.178 and 0.261. By the fact that  $\|\bar{f}''\|_\infty \leq 1.332$ , we have

$$\sup_{x \in [-10, 10]} |\bar{f}'(x)| \leq 0.261 + 1.332 \cdot 0.001 \leq 0.263.$$

It can be shown that  $\bar{f}'(x)$  diminishes when  $x \notin [-10, 10]$ .

Next, we evaluate the value of  $\bar{f}(x)$  for each  $x \in \mathcal{X}$ . The numerical results show that these values are between -0.229 and 0.315. By the fact that  $\|\bar{f}'\| \leq 0.263$ , we have

$$\sup_{x \in [-10, 10]} |\bar{f}(x)| \leq 0.315 + 0.263 \cdot 0.001 \leq 0.316.$$

It is easily seen that the value of  $\bar{f}(x)$  is negligible when  $x < -10$ . On the other hand, when  $x > 10$ , the value of  $\bar{f}(x)$  monotonically decreases and is bounded below by its asymptotic limit:  $\lim_{x \rightarrow \infty} \bar{f}(x) \geq -0.229$ .  $\square$

We provide the complete proof of Lemma 4 in the supplementary materials. Fig. 3 visually confirms the small deviations in both the function shapes and the derivatives of the two functions.

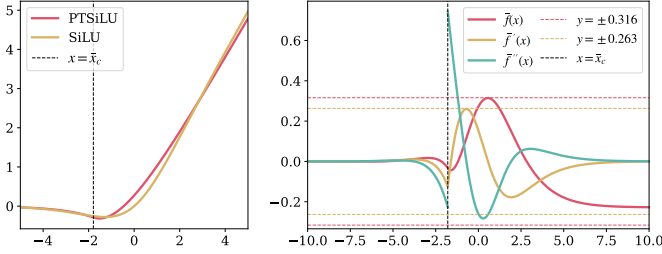


Fig. 3: *Left*: The PTSiLU and the SiLU function. *Right*: The bounds on the deviations between these two functions.

#### E. Training Process

As we adopted an ANN-to-SNN conversion method to obtain our SpikySpace, we first trained a quantized ANN model with PTsoftplus and PTSiLU as the activation functions and then converted it into an SNN model. Specifically, we followed BiT [34] and Sorbet [18] to quantize the activation into  $n$  bits. The quantization is in a Learned Step-size Quantization(LSQ) manner. Represented as:

$$X_Q = \alpha \cdot \text{clip}\left(\text{round}\left(\frac{X_R - \beta}{\alpha}\right), Q_n, Q_p\right) + \beta \quad (24)$$

We adopt a uniform quantization scheme with a learnable step size  $\alpha$  and an optional offset  $\beta$ . According to [34],  $\alpha$  can be initialized by

$$\alpha^* = \frac{\|\mathbf{X}_R \odot \mathbb{1}_{\{\mathbf{X}_R \geq 0.5\}}\|_1}{n_{\{\mathbf{X}_R \geq 0.5\}}} \quad (25)$$

and  $\beta$  can be initialized as 0. Straight-through estimator (STE) is employed as commonly used in previous works to back-propagate the gradients to  $\alpha$ .

This quantization method covers both symmetric and asymmetric cases. Specifically, the real-valued tensor  $X_R$  is first normalized by subtracting the offset  $\beta$  and dividing by  $\alpha$ . The result is rounded to the nearest integer and clipped to the representable integer range  $[Q_n, Q_p]$ , which is determined by the bit width  $b$ . Finally, the quantized value is mapped back to the real domain as  $X_Q$ . When  $\beta = 0$  and  $(Q_n, Q_p) = (-2^{b-1}, 2^{b-1} - 1)$ , the formulation reduces to symmetric quantization. When  $\beta \neq 0$  and  $(Q_n, Q_p) = (0, 2^b - 1)$ , It becomes asymmetric quantization.

We note that our quantization method inherently retains certain floating-point operations for the scaling factor  $\alpha$  and offset  $\beta$ . However, this does not pose a limitation, as prior studies [18] have shown that these parameters can be further quantized to power-of-two values, allowing multiplications to be replaced by efficient bit-shifting operations without noticeable accuracy degradation.

## V. EXPERIMENTAL EVALUATION

### A. Experimental Setups

1) *Dataset*: We evaluate our model on four widely used multivariate time series forecasting benchmarks, spanning diverse application domains including traffic, solar energy, and

electricity consumption. All datasets are divided chronologically into training, validation, and test sets without shuffling. The statistical details and split ratios are summarized in Table II.

- **METR-LA** [10]: Traffic speed data collected from 207 loop detectors on Los Angeles highways, aggregated every 5 minutes. The dataset contains 34,272 samples, each with a sequence length of 12 and 207 variables. It is split into training, validation, and test sets with a ratio of (0.7, 0.2, 0.1). This dataset captures strong spatial-temporal dependencies due to road network topology.
- **PEMS-BAY** [10]: Another large-scale traffic dataset from the California Bay Area, sampled every 5 minutes from 325 sensors. It includes 52,116 samples, each of length 12 with 325 variables. The chronological split ratio is (0.7, 0.2, 0.1). PEMS-BAY is widely adopted for benchmarking spatiotemporal forecasting models.
- **Solar-Energy** [11]: Solar power production recorded from 137 photovoltaic plants across several years, exhibiting strong daily and seasonal periodicity. The dataset contains 52,560 hourly samples with 137 variables and a sequence length of 168. It is partitioned into training, validation, and test sets with a ratio of (0.6, 0.2, 0.2).
- **Electricity** [11]: Hourly electricity consumption data from 321 clients over multiple years, showing clear diurnal and weekly patterns. The dataset includes 26,304 samples, each with 321 variables and a sequence length of 168. It is divided into train/validation/test sets in the ratio (0.6, 0.2, 0.2).

2) *Baselines*: We compare SpikySpace with the following time series forecasting methods, including both ANN and SNN baselines:

- **GRU** [35]: A recurrent neural network (RNN) model that captures temporal dependencies through gated recurrent units. It serves as a classical ANN baseline for sequence modeling.
- **iTransformer** [36]: A state-of-the-art transformer variant that learns both instance-wise and channel-wise dependencies in multivariate time series, representing strong ANN performance under full-precision computation.
- **SpikeTCN** [2]: A convolutional SNN that integrates temporal convolution with spike-based processing, highlighting the benefit of temporal feature extraction in event-driven computation.
- **SpikeRNN** [2]: A recurrent SNN model that replaces analog activations with spiking neurons, enabling energy-efficient sequential modeling through temporal dynamics.
- **iSpikformer** [2]: A spiking adaptation of the transformer architecture that replaces softmax attention and linear layers with spike-compatible modules, achieving competitive accuracy with reduced energy.
- **SpikeSTAG** [29]: A hybrid spatio-temporal graph SNN designed for structured time-series data, combining graph connectivity with event-driven updates to model spatial correlations efficiently.

TABLE I: Experimental results of time-series forecasting on four benchmarks with different prediction horizons ( $L$ ). The best and second-best results in **SNNs** are highlighted in bold and underlined, respectively.  $\uparrow$  ( $\downarrow$ ) indicates that higher (lower) values are better.

Dataset	Horizon	GRU		iTransformer		SpikeTCN		SpikeRNN		iSpikformer		SpikeSTAG		SpikySpace	
		$R^2 \uparrow$	RRSE $\downarrow$												
<b>Metr-la</b>	3	.803	.448	.864	.344	.845	.415	.784	.490	.805	.466	<b>.873</b>	<b>.375</b>	<b>.894</b>	<b>.343</b>
	6	.761	.507	.849	.410	.799	.473	.731	.547	.765	.512	<u>.822</u>	<u>.430</u>	<b>.848</b>	<b>.412</b>
	12	.682	.585	.763	.514	.718	.560	.661	.614	.723	.555	<u>.734</u>	<u>.535</u>	<b>.760</b>	<b>.517</b>
	24	.614	.663	.538	.652	.602	.665	.557	.702	.549	.709	<u>.590</u>	<u>.685</u>	<b>.610</b>	<b>.659</b>
	Avg.	.715	.551	.754	.480	.741	.528	.683	.588	.711	.561	<u>.755</u>	<u>.506</u>	<b>.778</b>	<b>.483</b>
<b>Pems-bay</b>	3	.783	.479	.938	.269	.862	.401	.763	.527	<b>.935</b>	<b>.276</b>	.874	.384	<b>.921</b>	<b>.304</b>
	6	.769	.504	.888	.362	.829	.448	.721	.571	<b>.884</b>	<b>.369</b>	.835	.439	<b>.866</b>	<b>.395</b>
	12	.696	.638	.797	.488	.782	<u>.504</u>	.710	.582	<b>.787</b>	<b>.499</b>	<u>.787</u>	.537	.762	.528
	24	.696	.638	.629	.659	<u>.681</u>	<b>.582</b>	<b>.693</b>	<u>.599</u>	.622	.665	.626	.661	.605	.683
	Avg.	.736	.565	.813	.444	.788	.484	.722	.570	<b>.807</b>	<b>.452</b>	.780	.505	.788	.478
<b>Solar</b>	3	.962	.508	.974	.562	.946	<u>.205</u>	.933	.246	<b>.972</b>	.217	<b>.973</b>	.246	.971	<b>.176</b>
	6	.950	.548	.964	.584	.937	.252	.923	.278	<b>.955</b>	<b>.218</b>	.950	.272	<b>.953</b>	<b>.223</b>
	12	.907	.569	.918	.575	.893	.409	.903	.343	<u>.918</u>	<b>.295</b>	<b>.926</b>	.315	.914	<b>.301</b>
	24	.875	.572	.879	.541	.840	.541	.820	.425	<u>.869</u>	<b>.372</b>	<b>.879</b>	<u>.390</u>	.821	.434
	Avg.	.924	.549	.934	.566	.904	.352	.895	.323	<u>.929</u>	<b>.275</b>	<b>.932</b>	.306	.915	<u>.284</u>
<b>Electricity</b>	3	.983	.518	.983	.213	.974	.324	.984	.207	.982	.214	<u>.987</u>	<u>.207</u>	<b>.994</b>	<b>.136</b>
	6	.981	.522	.977	.506	.970	.333	.978	.280	.974	.284	<u>.986</u>	<u>.222</u>	<b>.992</b>	<b>.157</b>
	12	.980	.531	.977	.460	.968	.338	.979	.314	.973	.284	<u>.985</u>	<u>.224</u>	<b>.990</b>	<b>.176</b>
	24	.972	.506	.977	.305	.963	.342	.964	.317	.974	.284	<u>.984</u>	<u>.225</u>	<b>.990</b>	<b>.179</b>
	Avg.	.979	.519	.978	.371	.969	.334	.976	.279	.976	.266	<u>.985</u>	<u>.220</u>	<b>.992</b>	<b>.162</b>

TABLE II: Statistics of the four benchmarks.

Dataset	# Samples	# Variables	Sample Rate	Length
Metr-la	34,272	207	5 minutes	12
Pems-bay	52,116	325	5 minutes	12
Solar	52,560	137	10 minutes	168
Electricity	26,304	321	1 hour	168

3) *Evaluation Metrics*: For evaluation, we reported the coefficient of determination ( $R^2$ ) and Root Relative Squared Error (RRSE) for each dataset across all the horizons. Let  $y_t$  denote the ground-truth value at time step  $t$ ,  $\hat{y}_t$  denote the corresponding model prediction, and  $\bar{y}$  denote the mean of all ground-truth values. The two metrics are defined as:

$$R^2 = 1 - \frac{\sum_t (y_t - \hat{y}_t)^2}{\sum_t (y_t - \bar{y})^2}, \quad (26)$$

$$\text{RRSE} = \sqrt{\frac{\sum_t (y_t - \hat{y}_t)^2}{\sum_t (y_t - \bar{y})^2}}, \quad (27)$$

A higher  $R^2$  indicates stronger goodness of fit, while a lower RRSE reflects smaller relative error and better cross-dataset comparability. We follow prior work in adopting these two metrics rather than MAE or MSE, since they are scale-

invariant and thus comparable across datasets with different magnitudes, and they better highlight both relative deviation and variance-explained quality.

4) *Implementation Details*: In all experiments, we set the batch size to 64 and the learning rate to  $5 \times 10^{-4}$ . For each dataset, the forecasting horizons are set to 3, 6, 12, and 24 time steps. Our model is trained using the Adam optimizer with the mean squared error (MSE) as the loss function. During training, we set the maximum epoch number as 1000 while the early stop patience as 20. All experiments are conducted on a single NVIDIA A100 GPU with 80GB of memory. The SpikySpace model results we reported in Table I are using a timestep  $T = 3$ , which means we use a spike train length as 3 to represent a scalar.

## B. Results

The evaluation results across four datasets and four prediction horizons for our models are shown in Table I. SpikySpace achieves the highest  $R^2$  and lowest RRSE values on two datasets and near best on the other two, demonstrating strong generalization and stability across different domains and horizons. In particular, on the Electricity dataset, SpikySpace achieves  $R^2 = 0.992$  and RRSE= 0.162, surpassing both iSpikformer and iTransformer while using fully spiking computation. On traffic datasets like Metr-la, SpikySpace attains

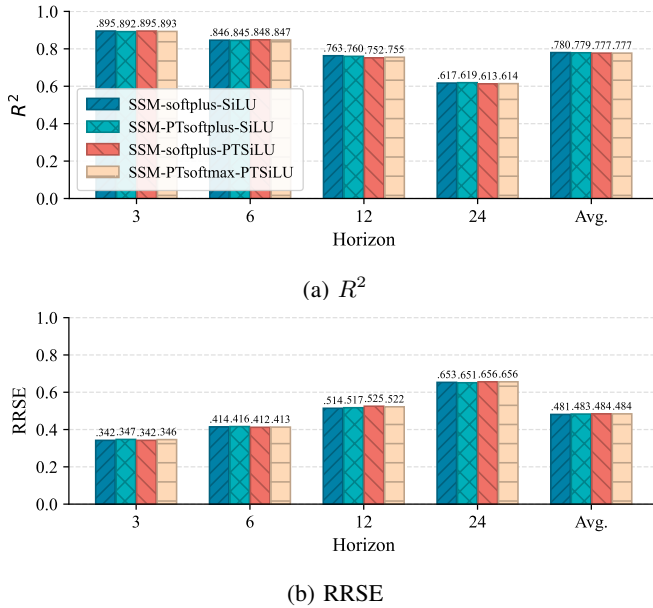


Fig. 4: Ablation study results of PTSoftplus and PTSiLU on full-precision ANNs.

Bits	PTsoftplus	PTSiLU	$R^2$	$\Delta R^2$
4	✗	✗	.607	N/A
	✓	✗	.611	+.004
	✗	✓	.611	+.004
	✓	✓	.610	+.003
1	✗	✗	.612	N/A
	✓	✗	.605	-.007
	✗	✓	.616	+.004
	✓	✓	.603	-.009

TABLE III: Ablation study on the impact of PTsoftplus and PTSiLU. ‘Bits’ in this table denotes the activation quantization bit-width.

$R^2$  gains of 2.3% respectively over the strongest SNN baselines, confirming that its selective scan mechanism effectively captures temporal dependencies under sparse updates. On the other two datasets, SpikySpace’s performance remains competitive with a smaller model size and less energy consumption. These results demonstrate that SpikySpace closes the accuracy gap between SNNs and dense ANNs while maintaining neuromorphic efficiency.

### C. Ablation Study

To better understand the contribution of each component in SpikySpace, we conducted a comprehensive ablation study focusing on the proposed activation approximations and the effect of timestep selection on forecasting performance.

1) *Approximated Operations*: To assess the effectiveness of the proposed PTsoftplus and PTSiLU activations, we conduct a controlled ablation against their full-precision counterparts. As shown in Fig. 4, replacing the standard Softplus and

SiLU with our power-of-two variants achieves almost identical accuracy across all forecasting horizons, confirming that the approximations retain the expressive capacity of the original functions.

We then quantifies this effect under different activation bit-widths as shown in Table III. At 4-bit precision, both PTsoftplus and PTSiLU yield a small gain of  $\Delta R^2 = +0.004$ , and their combination results in only  $+0.003$  deviation from the Softplus–SiLU baseline. Even at 1-bit quantization, the accuracy drop remains below 1% ( $\Delta R^2 = -0.009$ ), showing strong robustness to coarse quantization.

Overall, PTsoftplus and PTSiLU preserve smooth gating and differentiability while enabling efficient bit-shift implementations without costly exponentials or divisions.

2) *Timestep*: In the main results shown in Table I, we adopted the  $T=3$  for the SpikySpace model, converted from the 2-bit activation ANNs. This setting provides a good balance between temporal resolution and computational efficiency in the selective scan.

To further analyze its impact, we conduct an ablation study by varying the internal timestep  $T$  while keeping all other configurations identical and the results are shown in Table IV.

Overall, changing  $T$  has little influence on forecasting accuracy across datasets and horizons, indicating that the discrete-time state evolution of SpikySpace is stable under different update granularities. However, when the timestep is reduced to  $T=1$ , we observe a few undesired results on Metr-la at larger horizons. To avoid these rare but suboptimal behaviors, we adopt  $T=3$  for all reported experiments.

### D. Energy Analysis

Unlike traditional deep networks, the energy consumption of an SNN is primarily determined by the time-window length  $T$  and the spike rate  $s$  [37]. In a conventional ANN, a neuron performs one MAC operation as  $y = w \cdot x$ . If we encode  $x$  to spike train, which only consist 0s and 1s, we can replace the MACs with simpler ACCs and thus save energy. For example,  $x = 2/3$  can be encoded as  $[1, 1, 0]$  with  $T = 3$ . The two 1s indicates adding the weight twice. Mathematically, the ACC operations in SNN scales linearly with the total spike count, approximately  $T \cdot s$  times.

In our spiking state-space models, as presented in Eq. 13, the transition matrix  $\bar{\mathbf{A}}_t$  introduces a positive values and accumulates through time propagates, reaching the clamping maximum and leading to a spike rate toward  $\sim 100\%$ . In this case, spike will occur at every time step and the spike train will consist of all 1s and no 0s. To address this, we scale the firing threshold as  $\theta' = T \cdot \theta$ , so that according to the spiking algorithm showing in Algorithm 1, the  $T$  spikes in the spike train collapses to a single spike, reducing the spike rate from 1 to  $1/T$ . To preserve the overall signal magnitude, we also scale the weights by  $T$  like  $\mathbf{W}' = T \cdot \mathbf{W}$ , which keeps the output numerically consistent with the unscaled case.

With this notice, we reduce the average spike rate from 93% to 26.8%, yielding an average energy of  $0.12 \text{ mJ}$  on the Electricity dataset with a horizon of 3.

TABLE IV: Ablation study results on timesteps. Tested across two datasets and all 4 horizons.

Dataset	Horizon	1		3		7		15	
		$R^2\uparrow$	$RRSE\downarrow$	$R^2\uparrow$	$RRSE\downarrow$	$R^2\uparrow$	$RRSE\downarrow$	$R^2\uparrow$	$RRSE\downarrow$
Solar	3	0.971	0.176	0.971	0.176	0.970	0.179	0.969	0.181
	6	0.952	0.225	0.952	0.224	0.949	0.232	0.946	0.239
	12	0.911	0.306	0.913	0.302	0.905	0.317	0.904	0.318
	24	0.833	0.420	0.821	0.434	0.830	0.424	0.838	0.413
Metr-la	3	0.894	0.344	0.894	0.343	0.894	0.343	0.895	0.343
	6	0.847	0.413	0.848	0.412	0.847	0.413	0.847	0.413
	12	0.757	0.520	0.760	0.517	0.759	0.518	0.758	0.519
	24	0.604	0.664	0.610	0.659	0.608	0.661	0.613	0.656

TABLE V: Comparison of the model size, energy consumption, and performance across SpikySpace and baselines. The energy reduction is calculated relative to that of iTransformer. The measurements are based on the Electricity dataset with a prediction horizon of 3.

Model	Backbone	SNN	Param (M)	Energy (mJ)	Energy Reduction	$R^2\uparrow$	$RRSE\downarrow$
SpikySpace	SSM	✓	0.868	0.12	98.73%	0.994	0.136
SpikeSTAG	LSTM, transformer	✓	1.566	4.39	53.64%	0.987	0.207
iSpikformer	transformer	✓	1.634	3.19	66.30%	0.982	0.214
iTransformer	transformer	✗	1.634	9.47	/	0.983	0.213

The parameter size and energy consumption of our SpikySpace are shown in Table V. Compare with the state-of-the-art models, the parameter size of our model is about 53.1% to 55.4% while reduces estimated energy consumption by 98.73% and 96.24% compared to iTransformer and iSpikformer, respectively.

## VI. DISCUSSION

### A. Neuromorphic Compatibility

While current neuromorphic hardware platforms are still under active development and not yet widely accessible, we assess the hardware compatibility of SpikySpace by implementing the core computational operators within the Lava framework, targeting Intel’s Loihi architecture. These implementations verify that our proposed operations can be effectively mapped to existing neuromorphic substrates.

Although we map the model onto 45nm technology to obtain the energy cost [38], these analyses do not fully capture hardware-level dynamics such as routing delay, synaptic buffering, or spike serialization overhead. Future work will focus on deploying SpikySpace on real neuromorphic platforms like Loihi [39] or BrainScaleS-2 [40] to obtain empirical latency and power measurements, validate our simulation assumptions, and enable further hardware-aware optimizations.

### B. Forecasting Horizon

We observe that SpikySpace achieves superior accuracy at shorter forecasting horizons like 3, 6, and 12 steps, but the performance gain diminishes when the horizon came to 24 steps, especially for the Metr-la and Pems-bay datasets. We attribute this to the design of the state-space formulation. In

multi-step forecasting, small prediction errors may accumulate across steps. Since SpikySpace updates its latent state through compact linear transitions without global re-contextualization, these accumulated deviations are not explicitly corrected.

Despite this limitation at longer horizons, strong performance on short forecasting horizons remains highly valuable in many real-world applications. In domains such as real-time traffic flow control, renewable energy regulation, and edge-based anomaly detection, the ability to deliver fast and energy-efficient short-term predictions is often more critical than maximizing long-horizon accuracy.

## VII. CONCLUSION

In this paper, we presented SpikySpace, the first fully spiking state space model that enables sparse, event-driven state updates by reformulating state-space dynamics into a spike-driven selective scan. Designed for energy-efficient time-series forecasting, SpikySpace extends the spiking paradigm beyond conventional recurrent or transformer structures, establishing a principled framework for neuromorphic sequence modeling.

To support spiking SSMs, we further proposed PTsoftplus and PTSiLU. These two functions serve as the counterparts of conventional Softplus and SiLU activations, achieving both computational efficiency and biological plausibility. Evaluated on four benchmarks of time series forecasting, SpikySpace achieved performance comparable to state-of-the-art models with substantial energy savings.

## AI-GENERATED CONTENT ACKNOWLEDGMENT

This manuscript made limited use of ChatGPT (GPT-5 2025) solely for language polishing to enhance readability and grammar. The tool was not used in drafting or revising any scientific content, including conceptual development, technical descriptions, data analysis, figures, or conclusions. All scientific content was developed and verified by the authors.

## REFERENCES

- [1] K. Yamazaki, V.-K. Vo-Ho, D. Bulsara, and N. Le, “Spiking neural networks and their applications: A review,” *Brain sciences*, vol. 12, no. 7, p. 863, 2022.
- [2] C. Lv, Y. Wang, D. Han, X. Zheng, X. Huang, and D. Li, “Efficient and effective time-series forecasting with spiking neural networks,” *arXiv preprint arXiv:2402.01533*, 2024.
- [3] F. SHIBO, W. Feng, X. Gao, P. Zhao, and Z. Shen, “Ts-lif: A temporal segment spiking neuron network for time series forecasting,” in *The Thirteenth International Conference on Learning Representations*, 2025.
- [4] A. Gu, K. Goel, and C. Ré, “Efficiently modeling long sequences with structured state spaces,” *arXiv preprint arXiv:2111.00396*, 2021.
- [5] A. Gu and T. Dao, “Mamba: Linear-time sequence modeling with selective state spaces,” in *First Conference on Language Modeling*, 2024.
- [6] S. Shen, C. Wang, R. Huang, Y. Zhong, Q. Guo, Z. Lu, J. Zhang, and L. Leng, “Spikingssms: Learning long sequences with sparse and parallel spiking state space models,” in *Proceedings of the AAAI Conference on Artificial Intelligence*, vol. 39, no. 19, 2025, pp. 20380–20388.
- [7] M. Bal and A. Sengupta, “P-spikessm: Harnessing probabilistic spiking state space models for long-range dependency tasks,” *arXiv preprint arXiv:2406.02923*, 2024.
- [8] Y. Zhong, R. Zhao, C. Wang, Q. Guo, J. Zhang, Z. Lu, and L. Leng, “Spike-ssm: A sparse, precise, and efficient spiking state space model for long sequences learning,” *arXiv preprint arXiv:2410.17268*, 2024.
- [9] Y. Huang, J. Tang, C. Wang, Z. Wang, J. Zhang, Z. Lu, B. Cheng, and L. Leng, “Spikingmamba: Towards energy-efficient large language models via knowledge distillation from mamba,” *arXiv preprint arXiv:2510.04595*, 2025.
- [10] Y. Li, R. Yu, C. Shahabi, and Y. Liu, “Diffusion convolutional recurrent neural network: Data-driven traffic forecasting,” in *International Conference on Learning Representations*, 2018.
- [11] G. Lai, W.-C. Chang, Y. Yang, and H. Liu, “Modeling long-and short-term temporal patterns with deep neural networks,” in *The 41st international ACM SIGIR conference on research & development in information retrieval*, 2018, pp. 95–104.
- [12] A. Taherkhani, A. Belatreche, Y. Li, G. Cosma, L. P. Maguire, and T. M. McGinnity, “A review of learning in biologically plausible spiking neural networks,” *Neural Networks*, vol. 122, pp. 253–272, 2020.
- [13] C. Zhou, H. Zhang, L. Yu, Y. Ye, Z. Zhou, L. Huang, Z. Ma, X. Fan, H. Zhou, and Y. Tian, “Direct training high-performance deep spiking neural networks: a review of theories and methods,” *Frontiers in Neuroscience*, vol. 18, p. 1383844, 2024.
- [14] C. Zhou, L. Yu, Z. Zhou, H. Zhang, Z. Ma, H. Zhou, and Y. Tian, “Spikingformer: Spike-driven residual learning for transformer-based spiking neural network,” *arXiv preprint arXiv:2304.11954*, 2023.
- [15] K. Tang, Z. Yan, and W.-F. Wong, “Onespike: Ultra-low latency spiking neural networks,” in *2024 International Joint Conference on Neural Networks (IJCNN)*. IEEE, 2024, pp. 1–8.
- [16] Y. Hu, Q. Zheng, X. Jiang, and G. Pan, “Fast-snn: Fast spiking neural network by converting quantized ann,” *IEEE Transactions on Pattern Analysis and Machine Intelligence*, vol. 45, no. 12, pp. 14 546–14 562, 2023.
- [17] R.-J. Zhu, Z. Wang, L. Gilpin, and J. Eshraghian, “Autonomous driving with spiking neural networks,” *Advances in Neural Information Processing Systems*, vol. 37, pp. 136 782–136 804, 2024.
- [18] K. Tang, Z. Yan, and W.-F. Wong, “Sorbet: A neuromorphic hardware-compatible transformer-based spiking language model,” *arXiv preprint arXiv:2409.15298*, 2024.
- [19] R. Nau, “Introduction to arima: nonseasonal models,” 2020. [Online]. Available: <https://people.duke.edu/~rnau/411arim.htm>
- [20] ———, “Moving average and exponential smoothing models,” 2020. [Online]. Available: <https://people.duke.edu/~rnau/411avg.htm>
- [21] R. C. Staudemeyer and E. R. Morris, “Understanding lstm – a tutorial into long short-term memory recurrent neural networks,” 2019. [Online]. Available: <https://arxiv.org/abs/1909.09586>
- [22] J. Chung, C. Gulcehre, K. Cho, and Y. Bengio, “Empirical evaluation of gated recurrent neural networks on sequence modeling,” 2014. [Online]. Available: <https://arxiv.org/abs/1412.3555>
- [23] C. Lea, M. D. Flynn, R. Vidal, A. Reiter, and G. D. Hager, “Temporal convolutional networks for action segmentation and detection,” 2016. [Online]. Available: <https://arxiv.org/abs/1611.05267>
- [24] H. Zhou, S. Zhang, J. Peng, S. Zhang, J. Li, H. Xiong, and W. Zhang, “Informer: Beyond efficient transformer for long sequence time-series forecasting,” 2021. [Online]. Available: <https://arxiv.org/abs/2012.07436>
- [25] H. Wu, J. Xu, J. Wang, and M. Long, “Autoformer: Decomposition transformers with auto-correlation for long-term series forecasting,” 2022. [Online]. Available: <https://arxiv.org/abs/2106.13008>
- [26] Y. Nie, N. H. Nguyen, P. Sinthong, and J. Kalagnanam, “A time series is worth 64 words: Long-term forecasting with transformers,” 2023. [Online]. Available: <https://arxiv.org/abs/2211.14730>
- [27] Y. Cheng, D. Wang, P. Zhou, and T. Zhang, “A survey of model compression and acceleration for deep neural networks,” 2020. [Online]. Available: <https://arxiv.org/abs/1710.09282>
- [28] C. Lv, D. Han, Y. Wang, X. Zheng, X. Huang, and D. Li, “Advancing spiking neural networks for sequential modeling with central pattern generators,” *Advances in Neural Information Processing Systems*, vol. 37, pp. 26 915–26 940, 2024.
- [29] B. Hu, C. Lv, M. Li, Y. Liu, X. Zheng, F. Zhang, F. Zhang *et al.*, “Spikestag: Spatial-temporal forecasting via gnn-snn collaboration,” *arXiv preprint arXiv:2508.02069*, 2025.
- [30] E. O. Neftci, H. Mostafa, and F. Zenke, “Surrogate gradient learning in spiking neural networks,” 2019. [Online]. Available: <https://arxiv.org/abs/1901.09948>
- [31] T. Bu, W. Fang, J. Ding, P. Dai, Z. Yu, and T. Huang, “Optimal ann-snn conversion for high-accuracy and ultra-low-latency spiking neural networks,” 2023. [Online]. Available: <https://arxiv.org/abs/2303.04347>
- [32] K. Yamazaki, V.-K. Vo-Ho, D. Bulsara, and N. Le, “Spiking neural networks and their applications: A review,” *Brain sciences*, vol. 12, no. 7, p. 863, 2022.
- [33] Z. Yan, K. Tang, J. Zhou, and W.-F. Wong, “Low latency conversion of artificial neural network models to rate-encoded spiking neural networks,” *IEEE Transactions on Neural Networks and Learning Systems*, 2025.
- [34] Z. Liu, B. Oguz, A. Pappu, L. Xiao, S. Yih, M. Li, R. Krishnamoorthi, and Y. Mehdad, “Bit: Robustly binarized multi-distilled transformer,” *Advances in neural information processing systems*, vol. 35, pp. 14 303–14 316, 2022.
- [35] K. Cho, B. van Merriënboer, Ç. Gülcöhre, D. Bahdanau, F. Bougares, H. Schwenk, and Y. Bengio, “Learning phrase representations using rnn encoder-decoder for statistical machine translation,” in *Proceedings of the 2014 Conference on Empirical Methods in Natural Language Processing (EMNLP)*, 2014, pp. 1724–1734.
- [36] Y. Liu, T. Hu, H. Zhang, H. Wu, S. Wang, L. Ma, and M. Long, “itransformer: Inverted transformers are effective for time series forecasting,” in *The Twelfth International Conference on Learning Representations*.
- [37] Z. Yan, Z. Bai, and W.-F. Wong, “Reconsidering the energy efficiency of spiking neural networks,” *arXiv preprint arXiv:2409.08290*, 2024.
- [38] M. Horowitz, “1.1 computing’s energy problem (and what we can do about it),” in *2014 IEEE international solid-state circuits conference digest of technical papers (ISSCC)*. IEEE, 2014, pp. 10–14.
- [39] M. Davies, N. Srinivasa, T.-H. Lin, G. Chinya, Y. Cao, S. H. Choday, G. Dimou, P. Joshi, N. Imam, S. Jain *et al.*, “Loihi: A neuromorphic manycore processor with on-chip learning,” *Ieee Micro*, vol. 38, no. 1, pp. 82–99, 2018.
- [40] C. Pehle, S. Billaudelle, B. Cramer, J. Kaiser, K. Schreiber, Y. Stradmann, J. Weis, A. Leibfried, E. Müller, and J. Schemmel, “The brainscales-2 accelerated neuromorphic system with hybrid plasticity,” *Frontiers in Neuroscience*, vol. 16, p. 795876, 2022.